Experimental Detection and Theoretical Characterization of Germanium-Doped Lithium Clusters Li_nGe ($n = 1-7$)

Vu Thi Ngan,[†,§] Jorg De Haeck,[‡,§] Hai Thuy Le,[‡,§] G. Gopakumar,[†] Peter Lievens,*[,‡,§] and Minh Tho Nguyen*[,†,§]

Department of Chemistry, Laboratory of Solid State Physics and Magnetism, and INPAC-Institute for Nanoscale Physics and Chemistry, Katholieke Universiteit Leuven, B-3001 Leuven, Belgium

Received: June 17, 2009; Revised Manuscript Received: June 23, 2009

We report a combined experimental and quantum chemical study of the small neutral and cationic germanium-doped lithium clusters $Li_nGe^{0,+}$ ($n = 1-7$). The clusters were detected by time-of-flight mass spectrometry after laser vaporization and ionization. The molecular geometries and electronic structures of the clusters were investigated using quantum chemical calculations at the DFT/B3LYP and CCSD(T) levels with the aug-cc-pVnZ basis sets. While $Li_3Ge^{0,+}$ and Li_4Ge^+ prefer planar structures, the clusters from Li_4Ge to Li_7Ge and the corresponding cations (except Li_4Ge^+) exhibit nonplanar forms. Clusters having from 4 to 6 valence electrons prefer high spin structures, and low spin ground states are derived for the others because valence electron configurations are formed by filling the electron shells 1s/1p/2s/2p based on Pauli's and Hund's rules. Odd−even alternation is observed for both neutral and cationic clusters. Because of the closed electronic shells, the 8- and 10-electron systems are more stable than the others, and the 8-electron species (Li_4Ge, Li_5Ge^+) are more favored than the 10-electron ones (Li_6Ge, Li_7Ge^+). This behavior for Ge is different from C in their doped Li clusters, which can be attributed to the difference in atomic radii. The averaged binding energy plot for neutrals tends to increase slowly with the increasing number of Li atoms, while the same plot for cations shows a maximum at Li_5Ge^+, which is in good agreement with the mass spectrometry experiment. Atom-in-molecules (AIM) analysis suggests that Li atoms do not bond to one another but through Ge or pseudoatoms, and an essentially ionic character can be attributed to the cluster chemical bonds. An interesting finding is that the larger clusters have the smallest adiabatic ionization energies known so far ($IE_a \approx 3.5$ eV).

1. Introduction

Lithium is the lightest metallic element and has often been used as a simple model to approach the electronic structure of heavier metals. The existence of their atomic aggregates larger than the dimer was demonstrated back in the mid 1970s.[1] Atomization energies of the dimer Li_2 and trimer Li_3 were thus determined making use of the Knudsen-effusion mass spectrometric techniques.[1] Evidence for the existence of the tetramer Li_4 and its thermochemical properties were subsequently reported.[1,2] Optical absorption spectra of small clusters from Li_4 to Li_8 were measured using depletion spectroscopy.[3] Subsequently, the dissociation pathways and binding energies of the larger and energy-rich cationic Li_n^+ clusters ($n = 4-42$) were determined from evaporation mass spectrometric experiments.[4] Thanks to their relatively small size, lithium clusters have been the subject of a large number of theoretical studies using a variety of quantum chemical methods.[5] From a more conceptual point of view, the cyclic electron delocalization in the planar hexamer Li_6 is relevant in the context of the σ-aromaticity of cyclic compounds.[6]

Since the experimental detection of the stable oxides and carbides of the type Li_3O[7] and Li_6C,[8] the Li clusters mixed with other elements have also attracted considerable interest. Although clusters doped by boron Li_nB,[9] oxygen Li_nO,[10] aluminum Li_nAl,[11] carbon Li_nC,[12] and tin Li_nSn[13] have theoretically been investigated, relevant experimental information is rather scarce. Using time-of-flight mass spectrometric (TOF-MS) techniques coupled with a laser vaporization source, some of us earlier have produced the lithium monoxides Li_nO ($2 \le n \le 70$)[14] and lithium monocarbides Li_nC ($n \le 70$)[15] and subsequently measured their ionization energies. These results provided thus evidence for the greater importance of rigid geometrical structures over metal-like characteristics for the small clusters. In the course of our current experimental studies in which the binary clusters Li_nGe_m containing both lithium and germanium atoms were produced by a dual-target dual-laser vaporization source,[16] we were able to identify the cationic monogermanides Li_nGe^+. Recently, some aspects of electronic distribution of the small neutral clusters Li_nGe ($n = 1-4$) have been examined theoretically.[17] In the present Article, we report the experimental observations of these clusters with $n = 1-7$, along with the results of a detailed theoretical investigation on their equilibrium geometries, electronic structures stabilities, and bonding properties.

2. Experimental and Computational Methods

Germanium-doped lithium clusters are experimentally produced using a dual-target dual-laser vaporization source.[16] Two rectangular targets of Ge and Li are placed beside each other and moved in a closed-loop pattern under computer control. The targets are exposed to the focused 532 nm laser light of two pulsed Nd:YAG lasers. Synchronous with the ablation of

* Corresponding author. E-mail: peter.lievens@fys.kuleuven.be (P.L.); minh.nguyen@chem.kuleuven.be (M.T.N.).
† Department of Chemistry.
‡ Laboratory of Solid State Physics and Magnetism.
§ INPAC.

10.1021/jp9056913 CCC: $40.75
Published on Web 07/21/2009

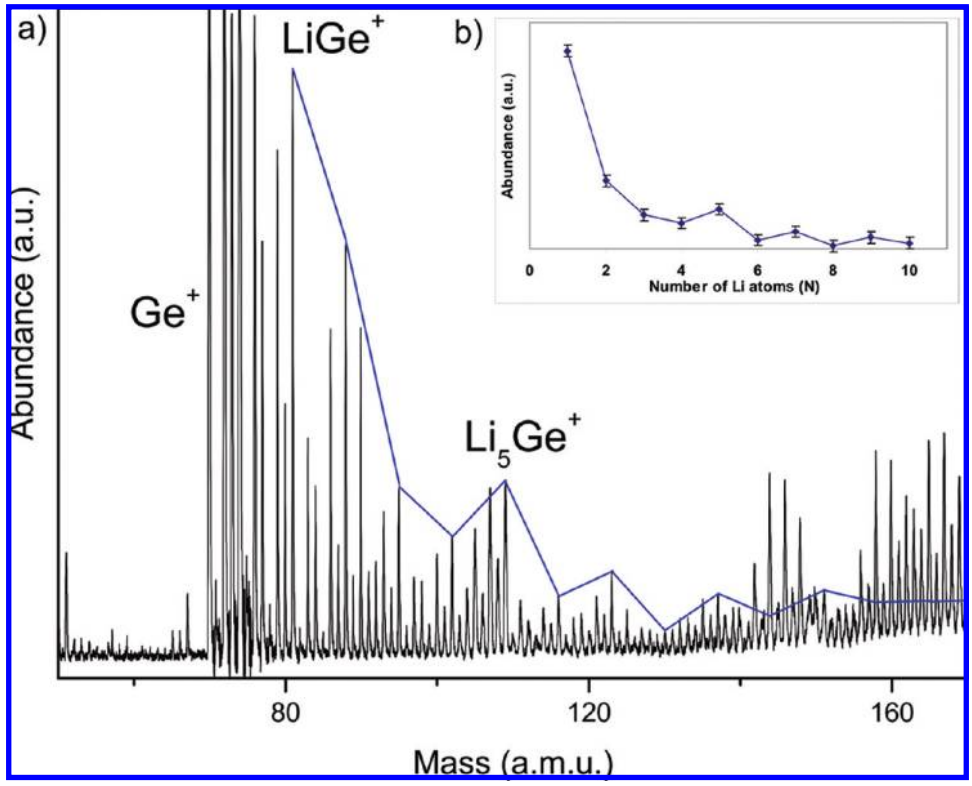

Figure 1. (a) RTOF mass abundance spectrum of Li_nGe^+ clusters, photodissociated by focused high fluence laser light from an ArF laser (6.4 eV). (b) Abundances of Li_nGe^+ clusters obtained by fitting the mass spectrum with isotope distributions for germanium- and oxygen-doped lithium clusters.

the target surfaces, helium gas is injected into the source by a pulsed gas valve, typically with a pressure of 5−6 bar. Cluster formation is initiated by collisions between atoms and clusters of the vaporized material and inert-gas atoms. The source is cooled to −40 °C by liquid nitrogen. The mixture of atoms, clusters, and inert gas undergoes a supersonic expansion into a vacuum chamber through a nozzle. The nozzle has a conical shape with an opening angle of 10°, and a throat diameter of 1.5 mm. The isentropic expansion reduces the temperature of the cluster beam and ends the cluster-growth process because of the rapidly decreasing density. The clusters are detected by a reflectron time-of-flight (RTOF) mass spectrometer ($M/\Delta M \approx 1000$). In the extraction region, clusters interact with focused high energy laser light (6.4 eV, ArF excimer laser) and absorb multiple photons, resulting in a considerable increase in excess energy. This leads to a significant probability of localizing enough internal energy to overcome the dissociation energy of a fragment or atom. As long as the free energy of the formed daughter fragments exceeds the binding energy of a constituent atom, this evaporation chain continues. Finally, the evaporation chain terminates at cluster configurations that are more stable than other cluster sizes at the same temperature. This results in the observation of stability patterns in the experimental mass spectrum.

Figure 1 shows a photodissociation mass spectrum of positively charged Ge-doped Li clusters. The highest peaks corresponding to Li_nGe^+ are connected by a solid line. The main features are the abundance enhancement of Li_5Ge^+ and an odd−even staggering starting at Li_4Ge^+. Using simple electron counting rules, Li_5Ge^+ is conceived to have 8 delocalized electrons. This number corresponds with a magic number for the spherical shell model for metal clusters. The experimentally observed odd−even effect can be attributed to a stability enhancement for an even number of delocalized electrons and is related to a deformation driven degeneracy lifting of the electronic energy levels, with singly occupied electron levels having higher energy.[18]

A more detailed analysis of the abundances of the different cluster sizes has been performed by using a fitting procedure incorporating calculated isotope distributions for Ge- and O-doped lithium clusters in the given size range. Formation of oxide aggregates is hard to avoid for Li clusters and has been investigated and discussed elsewhere.[19,20] After dissociation, the main oxygen-containing species left in the mass spectrum are GeO^+ and Li_8GeO^+. Both Li and Ge have multiple stable isotopes, which need to be accounted for to deduce the abundances observed in the mass spectrum correctly. The error on the mass calibration is below 0.1 amu in this size range, rendering identification of all peaks unambiguous. The obtained abundances of Li_nGe clusters for sizes from $n = 1$ up to 10 are shown in the inset of Figure 1 (Figure 1b) and confirm the two observations discussed above.

Quantum chemical calculations were carried out for the two lowest spin multiplicities $M = 2S + 1$ for each cluster considered. During the search for structures, geometries of all possible forms were fully optimized making use of density functional theory with the popular hybrid B3LYP functional,[21] in conjunction with the all electron augmented correlation consistent basis set aug-cc-pVnZ[22] (with n = D, T, and Q, depending on the size of the species). For each spin manifold, geometry optimization was carried out with and without imposing symmetry on the different initial configurations. Harmonic vibrational frequencies were subsequently calculated to characterize the located stationary points as equilibrium structures having all real vibrational frequencies.

To calibrate the relative energies obtained from DFT/B3LYP methods, separate molecular orbital calculations were done on small clusters using the coupled cluster CCSD(T) method.[23] All

calculations were performed using the Gaussian 03 package.[24] To unravel the electronic structure, we have considered the atoms-in-molecules (AIM)[25] and electron localization function (ELF)[26] approaches, which are proved to be useful tools providing valuable information about the electron distribution and bonding in molecules. The electron densities were generated at the B3LYP/aug-cc-pVDZ level, and the AIM critical points were located with the AIM2000[27] program. The ELF was computed using the TopMod[28] set of program, subsequently plotting the isosurfaces with the graphical program gOpenMol.[29] The density of states (DOS) was then used to assign the contribution of atomic orbitals to the bonding. A natural population analysis (NPA) of some selected low-lying isomers of neutral and cationic clusters was also done to probe the bonding phenomena of clusters considered in the present study.

3. Results and Discussion

In the present theoretical analysis, spin contamination in Hartree−Fock wave functions can be regarded as small, as the expectation values of $\langle S^2 \rangle$ deviate slightly (∼0.1) from the exact values. The energy orderings of different states and the relative energies determined at the B3LYP and CCSD(T) levels show some small deviations in a few cases. In general, changes in relative energies in going from B3LYP to CCSD(T) with the same aug-cc-pVTZ basis set amount to less than 0.05 eV (1.2 kcal/mol). The deviations are larger in the cases of the doublet state of LiGe (0.24 eV) and the triplet state of the Li_4Ge rhombus (0.12 eV). For Li_2Ge^+, the energy of the $^4A_2$ state relative to the ground $^2\Pi_u$ state is 0.33, 0.31, and 0.31 eV at the B3LYP/aug-cc-pVnZ with n = D, T, Q, respectively, but this energy difference becomes very small with the CCSD(T) method; even the sign is reversed with the smaller basis set aug-cc-pVDZ (−0.0018 and −0.016 eV without and with ZPE corrections, respectively). Table 1 lists the calculated results for other cases.

Where the comparison is possible, the B3LYP functional predicts the same ground-state structure as the CCSD(T) method with a large basis set, and to keep the consistency of the analysis, its results are used in the following description of the systems considered. The energetic values mentioned hereafter refer to, unless otherwise stated, those obtained from B3LYP/aug-cc-pVTZ + ZPE calculations. Geometrical structures of the various states of the neutral and cationic $Li_nGe^{0,+}$, with $n = 2-7$, are summarized in Figure 2 with numbering ranging from 1 to 30, and their optimized coordinates are available in the Supporting Information.

LiGe and $LiGe^+$. The ground state of LiGe is a $^4\Sigma^-$ state with a bond length of 2.402 Å, while the $^2\Sigma^+$ state has a larger Li−Ge bond length of 2.595 Å and energetically lying 0.29 eV above the ground state. However, a larger doublet−quartet gap has been estimated at the CCSD(T) level, which amounts to 0.57, 0.53, 0.52 eV with the basis sets aug-cc-pVnZ, where n = D, T, and Q, respectively. The spin density plot (Figure S1) indicates that the unpaired electrons are mainly concentrated on Ge. This is in agreement with the frontier orbital analysis illustrated in the Supporting Information; that is, the three unpaired electrons are distributed over two π and one σ orbitals centered on Ge. NBO analysis of α-orbitals points out one bond mainly formed from 2s(Li) and $4p_z$(Ge) orbitals, and this bond is strongly polarized toward Ge due to the large partition of Ge (86%), while there is no bond arising from the β-orbitals. There is an apparent electron transfer from the 2s(Li) to $4p_z$(Ge) orbital, which characterizes a certain ionic Li−Ge bond (NBO positive charge on Li is 0.78 e, where e stands for electron). Thus, the shell 4p of Ge is half filled by receiving one electron from 2s(Li). This is confirmed by its natural electron configuration ([core]$4s^{1.97}4p^{2.79}4d^{0.02}$), and it partly accounts for stability in accordance with Hund's rule.

The $^2\Sigma^+$ state of LiGe is less polarized than the quartet due to the less positive charge on Li (0.49 e). A two-electron bond has been identified by NBO analysis, which implies that the doublet state bonding is more covalent than the quartet state.

Similarly, the cation $LiGe^+$ adopts the high spin lowest-lying state. The estimated singlet−triplet ($^1\Sigma^+ \leftarrow {}^1\Pi$) gap, which amounts to 0.24 eV (0.23 eV at CCSD(T)/aug-cc-pVQZ), is

TABLE 1: Relative Energies in eV of Minima of Neutral Li_nGe and Cationic Li_nGe^+ Clusters with Respect to the Corresponding Ground State[a]

			Li_nGe		Li_nGe^+	
cluster		sym	doublet	quartet	singlet	triplet
LiGe	0	$C_{\infty v}$	0.292	**0.000**	0.237	**0.000**
			0.568		0.328	
			0.528		0.249	
			0.515		0.226	
Li_3Ge	3	C_{2v}	**0.000**			
	4	C_{2v}		0.656		**0.000**
				0.609		
				0.677		
	5	D_{3h}			0.039	
					0.122	
					0.073	
					0.053	
	6	C_{3v}		0.826		0.537
				0.724		0.490
				0.804		0.541
				0.809		
Li_5Ge	16	C_{4v}	**0.000**		0.004	
	17	D_{3h}			**0.000**	
	18			1.285		
	19					1.180
Li_7Ge	26	C_{3v}	**0.000 (d)**		**0.000**	
	27	C_{2v}	0.196 (d)	0.565	0.380	0.762; 0.811 (d)
	28	D_{5h}			0.385	
	29	C_{3v}			0.388	
	30	C_{3v}		0.634		

			singlet	triplet	doublet	quartet
Li_2Ge	1	$D_{\infty h}$		**0.000**	**0.000**	
	2	C_{2v}	0.415	0.152	0.597	0.310
			0.410	0.042	0.593	−0.016
			0.402	0.106	0.635	0.045
			0.411	0.133	0.649	0.074
Li_4Ge	7	C_{2v}	**0.000**	0.758		
				0.844		
				0.886		
	8	D_{4h}			**0.000**	
	9	D_{2h}		0.593		
				0.758		
				0.803		
	10	C_{3v}				1.355
						1.205
						1.332
Li_6Ge	20	O_h	**0.000**		**0.000**	
	21		0.408		0.723	
	23			0.512		
	24					1.893
	25					1.905

[a] The energy of each state is shown at most with four levels in descending order: B3LYP/aug-cc-pVTZ, CCSD(T)/aug-cc-pVDZ, CCSD(T)/aug-cc-pVTZ, CCSD(T)/aug-cc-pVQZ. Relative energies were corrected by ZPE calculated at B3LYP/aug-cc-pVTZ, except for Li_7Ge with ZPE obtained at B3LYP/aug-cc-pVDZ. The (d) indicates a distorted structure from the corresponding symmetry.

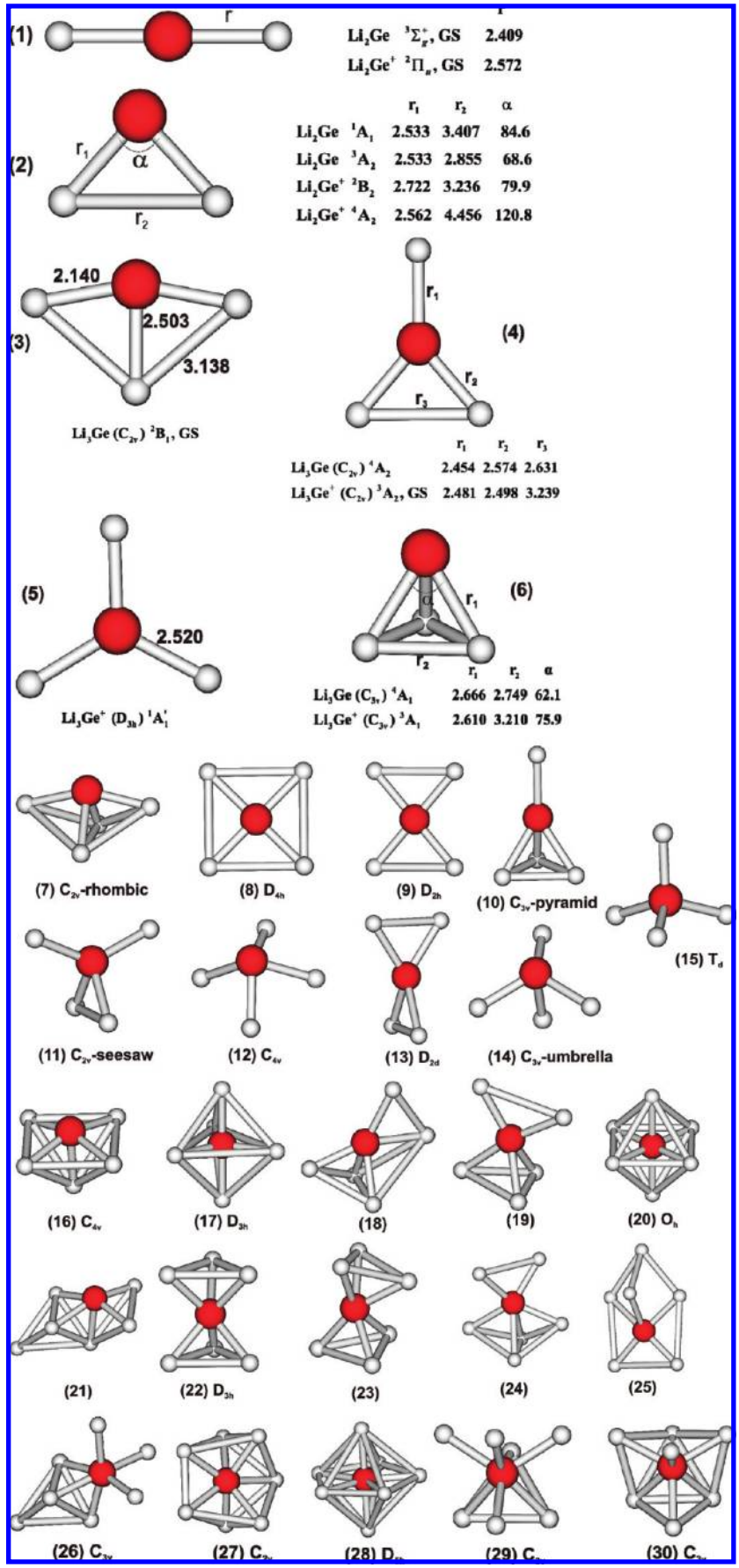

Figure 2. Selected geometries and shapes of the ground state and low-lying states of $Li_nGe^{0,+}$. Bond lengths are given in angstroms, and bond angles are in degrees (B3LYP/aug-cc-pVTZ).

rather small. The two unpaired electrons are located on Ge as can obviously be recognized from the spin density plot (Figure S1). The natural electron configurations of Li ([core]$2s^{0.09}2p^{0.03}$) and Ge ([core]$4s^{1.98}4p^{1.88}4d^{0.01}$) suggest that the $LiGe^+$ can best be regarded as a complex between a Ge atom and an Li^+ ion ($Ge\cdots Li^+$) with a long Li−Ge distance of 2.824 Å. The NBO positive charge is centered on Li with a value of 0.88 e as compared to 0.12 e on Ge. The ionization energy to remove one electron from the quartet LiGe to form the triplet $LiGe^+$ is 6.35 eV, which turns out to be the highest value in the series of the considered Ge-doped Li clusters.

Li_2Ge and Li_2Ge^+. We found two bent ($^1A_1$, $^3A_2$) and one linear ($^3\Sigma_g^-$) structure for Li_2Ge with the linear triplet as the electronic ground state. The bent $^3A_2$ state energetically lies 0.15 eV higher. The CCSD(T) single-point calculations reduce this value to 0.04, 0.11, and 0.13 eV with aug-cc-pVnZ basis sets, n = D, T, and Q, respectively. The $^1A_1$ state has higher energy content of 0.42 eV above $^3\Sigma_g^-$. The linear singlet structure is a transition state leading to the bent $^1A_1$ state.

A question of interest is why the linear structure is more stable than the bent one while the isovalent species GeH_2 is well-known having a bent structure. With this purpose in mind, we have plotted the density of state (DOS) for the $^3\Sigma_g^-$ state (Figure 3). Accordingly, the two degenerate singly occupied molecular orbitals (SOMO's) π_{ux}, π_{uy} are essentially stemming from $p_{x,y}$(Ge) and a small contribution of p(Li) orbitals. The next lower-lying MO (HOMO−2) is a bonding orbital (σ_u-type), which has large contributions of s(Li) and p_z(Ge). Here, the z-axis is chosen along the germanium and lithium atoms. Therefore, the bond primarily arises from the overlaps between $4p_z$(Ge) and 2s(Li) MO's. The extent of orbital overlap is larger at the linear geometry than the bent one. Hence, in the linear shape electrons are more easily transferred from Li to Ge. As a result, the positive charge on Li of the linear Li_2Ge (0.77 e) is larger than that of the bent Li_2Ge (0.50 e). The 4s(Ge) orbital lies much deeper than the 4p-orbitals and hardly decides the cluster structure. Note that in this case a high spin ground state is also more favored. Again, its origin can simply be understood by Hund's rule. At the triplet state, Hund's rule is satisfied, and the two degenerate π_{ux}, π_{uy} are singly occupied, thus leading to a maximum number of unpaired electrons.

For the Li_2Ge^+ cation, two bent ($^2B_2$, $^4A_2$) forms and one linear ($^2\Pi_u$) form are derived, with the linear doublet state being the lowest-lying. The $^4\Sigma_u^-$ state of linear geometry is a second-order saddle point (possessing a doubly degenerate imaginary frequency around 50i cm^{-1}), leading to the bent $^4A_2$ state, which is 0.31 eV less stable than the ground $^2\Pi_u$ state. Again, CCSD(T) calculations reduce the $^2\Pi_u-{}^4A_2$ gap to −0.016, 0.05, and 0.07 eV using the aug-cc-pVnZ basis sets with n = D, T, and Q, respectively. The very marginal $^2\Pi_u-{}^4A_2$ gap implies that the $^4A_2$ state is a competitive ground state of Li_2Ge^+. This may result from the competition between two factors affecting the stability of this cation: structure and spin state.

Dilithiated germanium favors a linear structure and high spin state as explained above. The ΔELF between the linear triplet neutral and vertical doublet cation of Li_2Ge (Figure S2) points out an electron movement from a delocalized π-orbital upon ionization. The ΔELF basin has large contributions from Ge.

Li_3Ge and Li_3Ge^+. We derived four different geometrical structures for trilithiated germanium: T-shape **3** (C_{2v}), isosceles triangle **4** (C_{2v}), equivalent triangle **5** (D_{3h}), and trigonal pyramid **6** (C_{3v}), and they are illustrated in Figure 2.

The D_{3h} structure **5** ($^2A_2''$), which is the corresponding ground state of Li_3C,[12] has been characterized as a second-order saddle point on the doublet PES of Li_3Ge and lying 0.12 eV higher than the T-shaped $^2B_1$ ground state. The imaginary frequency of the $^2A_2''$ state is a doubly degenerate E′ mode that corresponds to a combination of A_1 and B_2 modes within its largest Abelian subgroup C_{2v}. Upon lowering symmetry to the C_{2v} point group, two different structures were obtained: T-shape **3** and isosceles triangle **4**. The $^2B_1$ state of **4** is slightly distorted from the D_{3h} structure and has about the same energy content as the $^2A_2''$ state and still possesses one imaginary frequency (B_2 mode). The $^2B_1$ state of **3** is an energy minimum, which is the lowest-energy state of Li_3Ge. The $^4A_2$ state of structure **4** is a local minimum and is 0.66 eV less stable than the ground state. The trigonal pyramid C_{3v} **6** is a higher-energy local minimum in the $^4A_1$ state. However, the corresponding quartet state at the T-shaped geometry ($^4B_1$) has been characterized as a transition state with an imaginary B_2 vibrational mode. Overall, the neutral Li_3Ge thus adopts a T-shaped form **3** at its $^2B_1$ ground state.

A D_{3h} structure turns out to be a local minimum on the singlet potential energy surface of the cation. This can be interpreted by a decrease in internal repulsion when one electron is removed from the A_2'' orbital, which is perpendicular to the molecular plane. While the $^3B_1$ state of **3** has an imaginary frequency, the $^3A_2$ state of **4** is the global minimum on the Li_3Ge^+ PES, but it is just a little more stable (0.04 eV) than the D_{3h} structure. Besides, the $^3A_1$ state of the trigonal pyramid **6** is also a local minimum of Li_3Ge^+, which lies at 0.54 eV above the ground state.

ELF isosurfaces illustrated in Figure 4 for both neutral and cationic Li_3Ge indicate the presence of certain trisynaptic basins. The T-shaped ground state of Li_3Ge has two such trisynaptic basins V(Ge, Li1, Li2) and V(Ge, Li1, Li3), having the same electron population of 1.66 e. We were also able to locate two disynaptic basins V(Ge, Li2) and V(Ge, Li3), each having an electron population of 1.94 e. The population of one trisynaptic basin V(Ge, Li2, Li3) of the cation amounts to 3.56 e, and two equivalent disynaptic basins V(Ge, Li1) have a total population of 2.72 e. The existence of trisynaptic basins indicates the presence of three-center bonds in Li_3Ge that are absent in the linear Li_2Ge or the D_{3h} Li_3Ge.[17]

Li_4Ge and Li_4Ge^+. Reed et al.[30] found that, unlike the established tetrahedral structure of Li_4C, the isovalent Li_4X (X = Si, Ge, Sn) prefer a C_{2v} geometry analogous to that of SF_4. Geometries of tetralithiated germanium were optimized in the present work with and without imposing symmetry, at T_d, D_{4h}, C_{4v}, C_{3v}, and C_{2v} point groups considered in the two lowest spin states (singlet and triplet for the neutral, and doublet and quartet for the cation).

The global minimum of Li_4Ge is a C_{2v} open structure, which falls under the singlet manifold ($^1A_1$). It can be described as a Ge atom doped at the surface of the rhombus Li_4 unit **7** (C_{2v} rhombus). All other structures located on the singlet PES are saddle points. The C_{3v} umbrella structure **14** ($^1A_1$) is only 0.10 eV higher in energy but has a small doubly degenerate vibrational frequency (E mode of 37i cm^{-1}) whose motion is a triangular bending. The C_{4v} square pyramid **12** ($^1A_1$) is slightly less stable (0.10 eV) and has also an imaginary B_2 vibrational mode (77i cm^{-1}). Following the motion of this B_2 mode, a C_{2v}-rhombus structure is located. The D_{4h} **8** ($^1A_{1g}$) is a second-order saddle point; following its A_{2u} mode (116i cm^{-1}), a C_{4v} form is located, that is a transition state for interchanging the axial and equatorial position of lithium in the C_{2v} rhombus minimum. The B_{2u} mode (46i cm^{-1}) of **8** leads to the only minimum on the PES. T_d form **15** ($^1A_1$) is also located on the PES (relative energy being 0.25 eV), which has a triply degenerate imaginary

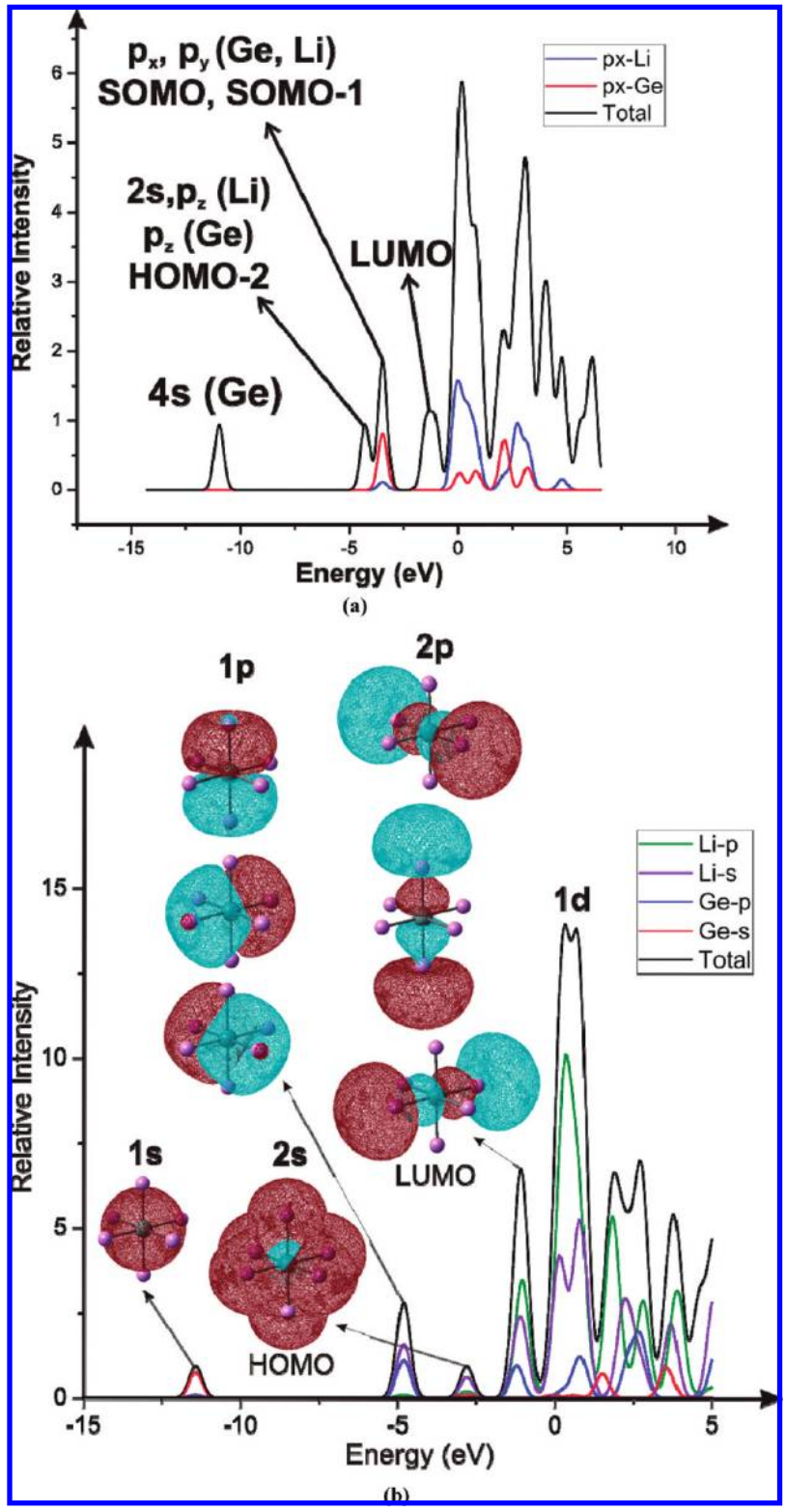

Figure 3. Density of states of (a) the linear triplet state Li_2Ge and (b) the singlet state of the octahedron Li_6Ge.

vibrational T_2 mode at 69i cm^{-1} leading to the C_{2v} rhombus as well. Therefore, all starting geometries invariably lead to the C_{2v} rhombus minimum on the singlet PES of Li_4Ge. This means that this isomer is very stable.

On the triplet PES, the two minima C_{2v} rhombus **7** and planar D_{2h} **9** have been located. The D_{2h} structure ($^3B_{3u}$) is the lowest-lying triplet form, but it lies at 0.59 eV above the singlet ground state. For the C_{2v} rhombus, an adiabatic singlet−triplet $^1A_1-^3B_1$ gap of 0.76 eV has been calculated. The stationary points **8** (D_{4h}) and **14** (C_{3v}) were not located as true minima on the PES. The former **8** ($^3A_{2u}$), which lies only 0.01 kcal mol^{-1} above the D_{2h} triplet, is a transition state for interchanging the position of two Li pairs of the D_{2h} triplet, whereas the latter **14** (C_{3v} umbrella, $^3A_1$) is a second-order saddle point and lies at 0.38 eV above the ground state.

The Li_4Ge^+ cation has a $^2A_{2u}$ lowest-lying state characterized by a D_{4h} square planar structure **8**. This can be obtained by optimizing from the rhombic structure of the neutral without

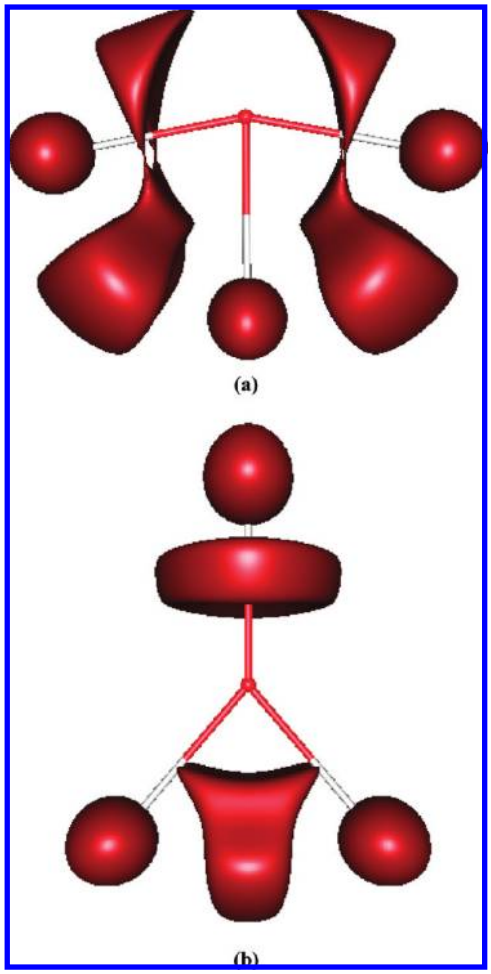

Figure 4. ELF isosurfaces of the ground state of (a) Li_3Ge and (b) Li_3Ge^+, with an isovalue of 0.80. The red ball is germanium atom; the gray balls are lithium atoms.

symmetry constraint. At lower symmetry, C_{2v} structures **11** were located in both doublet and quartet states, but with one and two imaginary frequencies, respectively. The Li_4Ge^+ quartet state bearing a C_{3v} pyramid structure (**10**, $^4A_1$) is found at 1.36 eV higher than the $^2A_{2u}$ ground state. Another high energy quartet minimum on the PES is having a D_{2d} form (**13**).

Interestingly, Li_4Ge does not adopt the tetrahedral structure like Li_4C. The reason for this can be found by analyzing their frontier MO's. This cluster has the following occupied valence MO's: the lowest-energy MO is an in-phase combination of 4s(Ge) and 2s(Li); the next three MO's are composed of 4p(Ge) and 2s(Li). The 2p(Li) AO's contribute to a lesser extent to all of the bonding MO's. The three main structures of Li_4Ge including tetrahedral T_d, squared D_{4h}, and rhombic C_{2v} forms all have the four MO's, which are shown in Figure 5 for the rhombic C_{2v}, but with different relative energies. The energies of the MO's not only depend on the structure but also on the bond lengths. The Ge−Li bond lengths in the three geometries stay almost the same (∼2.3−2.4 Å), but the Li−Li distances make the difference (3.850 Å in T_d, 3.313 Å in D_{4h}, and $Li_{ax}-Li_{eq} = 3.113$ Å, $Li_{eq}-Li_{eq} = 3.198$ Å in C_{2v}). This finally stems from a difference in atomic radii of carbon and germanium. Accordingly, the C_{2v} structure has the lowest orbital energies. The contribution of p(Li) AO's in C_{2v} form, which is larger than that in T_d form (16% vs 13%), is another reason accounting for the preference of the former.

Because of the relatively smaller radius of carbon, Li_4C adopts the T_d structure as the lowest-energy isomer. In this structure, the shorter Li−Li distances of 3.046 Å make the overlaps between orbitals of different Li atoms stronger than those in the T_d structure of Li_4Ge.

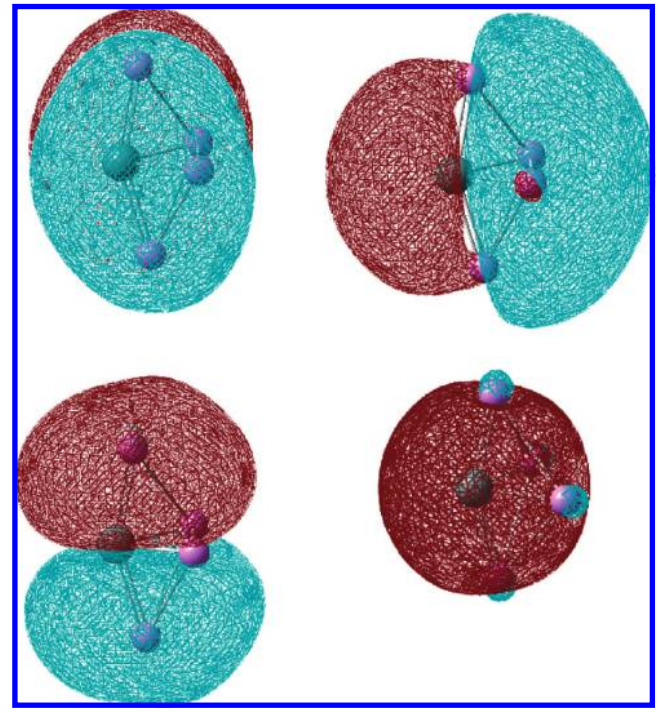

Figure 5. Frontier molecular orbitals of the ground electronic state of Li_4Ge with isosurface value of 0.01 au.

Li_5Ge and Li_5Ge^+. The most stable structure of Li_5Ge is obtained by subsequent addition of one Li atom to the Li_4Ge rhombus. This results in a $^2A_1$ state having a C_{4v} square pyramid form **16**. The D_{3h} structure **17** in which Ge occupies the center of a trigonal pyramidal Li_5 unit is a second-order saddle point (the imaginary E′ mode being ∼49i cm^{-1}) and lies 0.11 eV higher than **16**. This quantity can be considered as the energy barrier of a pseudorotation process. The quartet state of this cluster **18** lies at 1.29 eV above the doublet, and its structure can be described as a Li-capping on an edge of the Li_4Ge rhombus.

Upon removal of one electron from Li_5Ge, a D_{3h} cage structure ($^1A_1'$) is located as the lowest-lying state of Li_5Ge^+. However, the squared pyramidal $^1A_1$ state is calculated to be only 0.004 eV less stable than the D_{3h} structure. Within the expected accuracy of DFT calculations of ±0.2 eV, both D_{3h} **17** and C_{4v} **16** singlet structures are thus quasi degenerate and competitive for the ground state of this cation. Because of the very marginal energy barrier, the pseudorotation occurs very fast. This cation appears as the most pronounced peak in the photodissociation mass spectrum (Figure 1).

A triplet state minimum **19** is located at 1.18 eV above the lowest-energy singlet state. For both neutral and cationic pentalithiated germanium, high spin states are lying high relative to the corresponding low spin states.

Li_6Ge and Li_6Ge^+. The Li_6Ge was studied theoretically in the set of MX_6 compounds with M = C−Pb and X = Li−K.[31] The octahedral structure of Li_6Ge, as other clusters in the set, was found as a stable minimum. Here, we investigated all possible isomers of the neutral and cationic forms in different spin states.

Li_6Ge is confirmed to possess an O_h structure **20** in which the Ge atom is surrounded by six lithium atoms ($^1A_{1g}$). It is actually at this size that Ge becomes encapsulated in the lithium

cage while it occurs for the C atom already at Li_4C (T_d). Isomer **21** for Li_6Ge is described as a Li-capping to the trigonal face Li−Li−Li of the square pyramid Li_5Ge (C_s, $^1A'$), which is however 0.41 eV less stable. The triplet state of this cluster distorts from the D_{3h} **22** to the C_s **23** and lies at 0.51 eV higher than the singlet O_h **20**.

Removal of one electron from the $^1A_{1g}$ orbital of the Li_6Ge octahedron **20** results in a $^2A_{1g}$ state at the same point group, which is the cation ground state. A doublet state of Li_6Ge^+ having the form **21** (C_s, $^2A'$) and some quartet states **24**, **25** were also located, but they are much higher in energy.

Li_7Ge and Li_7Ge^+. Three different types of structure were found for both neutral and cationic heptalithiated germanium. The first **26** is a C_{3v} distorted octahedron capped by one Li on one face. The second **27** is a C_{2v} monocapped trigonal prism with encapsulated Ge. The third isomer **28** falls under the D_{5h} point group and possesses a pentagonal bipyramid structure with Ge in cage.

On the doublet PES of Li_7Ge, the lowest-energy form is distorted further from C_{3v} **26** in which Ge atom seems having six coordinates due to the long distance between the capped Li and Ge atom (4.612 Å). Another minimum being 0.20 eV less stable than the ground state was found to be distorted from C_{2v} **27**, in which Ge appears to be hepta-coordinated. The full C_{2v} structure **27** is a transition state on this doublet PES and energetically lying a little higher in energy (0.22 eV) than the corresponding distorted form. The C_{2v} pentagonal bipyramid, which is a distortion from D_{5h}, is not a local minimum as in the case for Li_7C reported in ref 12.

We were able to derive two low-lying quartet states with a hepta-coordinated Ge: the first is **27** (C_{2v}, $^4B_2$) and the second is **30** (C_{3v}, $^4A_1$), which are energetically lying at 0.56 and 0.63 eV, respectively, relative to the doublet ground state.

The lowest-lying state of Li_7Ge^+ is a $^1A_1$ state **26** (C_{3v}) having a coordination number of seven, because the bond length of 2.585 Å between capped Li and Ge is similar to other Li−Ge distances. Thus, both neutral and cationic forms of Li_7Ge have a similar ground structure **26**, even though the cation is more spherical than the neutral. Another C_{3v} isomer on the singlet PES has also been located for this cation, which is indeed geometrically similar to the hepta-coordinated isomer **29**, but it is located at 0.39 eV above the ground state. The full D_{5h} symmetric structure is also a minimum at 0.39 eV. One additional low-lying isomer identified on the singlet Li_7Ge^+ potential energy surface has a C_{2v} form **27** and lies at 0.38 eV higher than the ground state.

On the triplet PES, the two low-lying electronic states located include the C_{2v} **27** ($^3B_1$), which contains a hepta-coordinated Ge and lies at 0.76 eV above the singlet ground state. The second isomer is slightly distorted from the first one and is energetically lying a little higher than the first one (0.88 eV).

Ionization Energies, Bond Energies, and Stability. Table 2 lists the adiabatic ionization energies (IE_a) of Li_nGe calculated using B3LYP and CCSD(T) methods. It appears that the B3LYP/aug-cc-pVTZ level provides us with reliable values for this quantity. The most interesting finding is that the IE_a is significantly reduced with increasing number of Li atoms. The IE_a amounts to about ~3.5 eV for $n = 5-7$, which represents a so far smallest calculated value. These IEs of Li_nGe have values similar to those of Li_nC reported in ref 12 that were computed using the same functional and the smaller 6-311+G(d) basis set. While the absolute values of IE_a for $n = 2-4$ of Li_nGe are slightly higher than those of Li_nC, the IE_a values for $n = 5-7$ follow a reversed ordering. However, the trends of the whole series are similar. The smallest IE_a in the Li_nC series is 3.78 eV for $n = 7$, which is somewhat larger than the value of 3.52 eV of Li_7Ge. Note that the calculated IE_a of Li_7C was in good agreement with the experimental value (3.78 vs 3.69 eV). Nevertheless, the smallest experimental value was found for Li_5C (3.24 eV), which is rather far from the theoretical result (3.90 eV).[12]

TABLE 2: Lowest Adiabatic Ionization Energies of Li_nGe Clusters[a]

	IE_a (eV)				
N	B3LYP/ aVTZ	CCSD(T) aVDZ	CCSD(T) aVTZ	CCSD(T) aVQZ	change of geometry upon ionization
1	6.35	6.26	6.39	6.43	longer distances
2	5.23	5.05	5.14	5.17	linear, increased distance
3	4.73	4.50	4.57	4.55	T-shape → distorted D_{3h}
4	4.39	4.40	4.43		rhombic → square
5	3.77				square pyramid C_{4v} → D_{3h}
6	3.93				octahedron kept
7	3.52				distorted C_{3v} → C_{3v}

[a] IE_a evaluated from the ground states of neutral and cationic clusters Li_nGe at the B3LYP/aug-cc-pVTZ + ZPE level.

For a better understanding on the stability of the Ge-doped Li clusters, we have also calculated the averaged binding energy (E_b) and second difference energy (Δ^2E) of $Li_nGe^{0,+}$ clusters ($n = 1-7$) by the following formula:

$$E_b(Li_nGe) = [E_T(Ge) + nE_T(Li) - E_T(Li_nGe)]/n$$

$$E_b(Li_nGe^+) = [E_T(Ge) + (n-1)E_T(Li) + E_T(Li^+) - E_T(Li_nGe^+)]/n$$

$$\Delta^2E(Li_nGe) = E_T(Li_{n+1}Ge) + E_T(Li_{n-1}Ge) - 2E_T(Li_nGe)$$

$$\Delta^2E(Li_nGe^+) = E_T(Li_{n+1}Ge^+) + E_T(Li_{n-1}Ge^+) - 2E_T(Li_nGe^+)$$

where $E_T(X)$ stands for total energy of molecule X. Experimental results show a large increase of both Ge^+ and Li^+ in the photodissociation spectrum as compared to the ionization spectrum. Both signals are higher than the data threshold, but Li^+ is by far more abundant. Because Li is much more electropositive than Ge, the positive charge of the cationic clusters is expected to be concentrated on the Li atoms. Therefore, the averaged binding energies of cations are calculated on the basis of the processes:

$$Li_nGe^+ \rightarrow Ge + (n-1)Li + Li^+$$

To emphasize the size dependence for averaged binding and second difference energies of the clusters considered, the calculated results are tabulated as graphical representations shown in Figure 6. SOMO−LUMO energy gaps tabulated in Table 3 are also analyzed for gaining additional insights on the cluster stability. A positive value of averaged binding energy, which is calculated for both neutral and cationic clusters, suggests the existence of the considered clusters. The binding energies increase from $n = 1$ to 6 but the rates are relatively

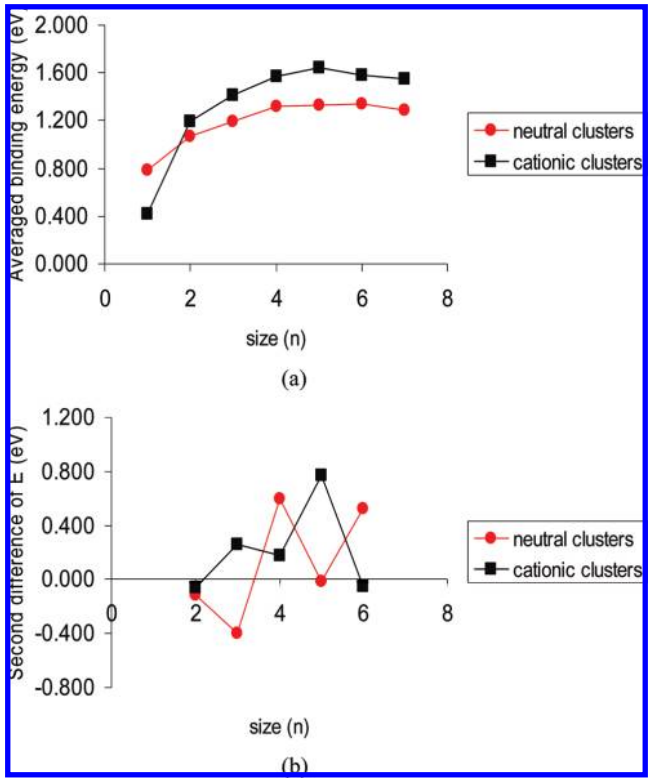

Figure 6. Size dependence of (a) the atomic binding energies and (b) the second difference of energies of Li_nGe and Li_nGe^+ ($n = 1-7$) clusters.

TABLE 3: HOMO(SOMO)−LUMO Energy Gaps (eV)[a] of Li_nGe and Li_nGe^+

n	neutral	cation
1	1.87	1.62
2	2.00	1.52
3	1.89	1.77
4	1.89	1.95
5	0.88	2.63
6	1.59	0.86
7[b]	1.09	2.06

[a] Values at the B3LYP/aug-cc-pVTZ level. [b] Values at the B3LYP/aug-cc-pVDZ level.

small, especially from $n = 4$ to 6. Interestingly, the averaged binding energy of cation shows a maximal value at Li_5Ge^+, which is in good agreement with the experimental mass spectrum (Figure 1).

The second difference of energies illustrated in Figure 6b shows the odd−even alternation of both neutrals and cations, which are more stable with an even number of electrons. The experiment (Figure 1) confirms that the even-electron cations have higher abundance than the odd-electron ones, especially for Li_5Ge^+ with 8 valence electrons. This means that the 10-electron species (Li_6Ge) are not particularly stable as in the case of C-doped lithium clusters,[12] but instead the 8-electron species (Li_4Ge, Li_5Ge^+) are.

A legitimate question is why Ge does behave so different from C. Let us inspect how the valence molecular orbitals are built up. The lowest-energy valence MO is derived from the in-phase overlap of 4s AO of C or Ge and 2s(Li). The three higher MO's are composed of each p-AO of C or Ge and the combination of 2s(Li). Filling these four MO's, we have 8-electron systems such as Li_4Ge, Li_5Ge^+, etc. The subsequent MO (the fifth one) is obtained by the out-of-phase combination

TABLE 4: Electron Density ($\rho(r_{BCP})$), Laplacian ($\nabla^2\rho(r_{BCP})$), Bond Ellipticity (ε), and Curvature λ_3 at Bond Critical Points of the Ground State of Neutral and Cationic $Li_nGe^{0,+}$ ($n = 1-5$) Clusters (B3LYP/aug-cc-pVDZ)

molecule	state	$\rho(r_{BCP})$	$\nabla^2\rho(r_{BCP})$	ε	λ_3
LiGe-quartet	$^4\Sigma$	0.02	0.02	0.00	0.13
$LiGe^+$-triplet		0.01	0.01	0.14	0.06
Li_2Ge	$^3\Sigma_g^+$	0.03	0.02	0.00	0.15
Li_2Ge^+	$^2\Pi_u$	0.02	0.02	0.08	0.12
Li_3Ge-T-shape	$^2B_1$				
BCP(Ge−Li1)		0.02	0.02	0.43	0.10
BCP(Ge−Li2,Li3)		0.02	0.03	0.16	0.14
Li_3Ge^+-C_{2v}	$^3A_2$				
BCP(Ge−Li1)		0.02	0.02	0.02	0.14
BCP(Ge−Li2,Li3)		0.02	0.02	0.09	
Li_4Ge-rhombic					
pseudo atom (Ps)		0.01	0.00	0.16	0.00
BCP(Li_{ax}−Ps)		0.01	0.00	0.21	0.01
BCP(Ge−Ps)		0.01	0.00	0.58	0.01
BCP(Ge−Li_{eq})		0.01	0.09	0.07	0.05
Li_4Ge^+-square	$^2A_{2u}$	0.02	0.02	0.17	0.14
Li_5Ge-C_{4v}	$^2A_1$				
BCP(Ge−Li_{ax})		0.02	0.02	0.00	0.11
BCP(Ge−Li_{eq})		0.02	0.02	0.00	0.13
Li_5Ge-D_{3h}	$^1A'_1$				
pseudo atom (Ps)		0.01	0.00	0.34	0.00
BCP(Li_{eq}−Ps)		0.01	0.00	0.19	0.01
BCP(Ge−Ps)		0.01	0.00	1.32	
BCP(Ge−Li_{ax})		0.02	0.02	0.00	0.12

of 4s of C or Ge and 2s(Li). In this MO, the overlaps between 2s(Li), if possible, are in-phase. The larger their overlap is, the lower is the MO energy. Because the atomic radius of Ge is much larger than that of C (1.25 vs 0.7 Å), the distance between lithium atoms in Li_nGe is significantly longer than that in Li_nC. Consequently, the in-phase overlaps in the fifth MO of Li_nGe are less than that of Li_nC, and then the energy gap between the fourth and fifth MO's of Li_nGe is larger than that of Li_nC. This is confirmed by the largest HOMO−LUMO gaps of 8-electron species Li_4Ge, Li_5Ge^+, while the 10-electron species Li_6C has the highest ionization energy within the Li_nC series.[12] In summary, the difference in atomic sizes is seemingly the original reason for the contrasting behavior between Ge and C in their doped lithium clusters.

Topology of Chemical Bonds. Because the derivatives of electron density such as the Laplacian, curvature, ellipticity, etc., contain a wealth of chemical information, we used the AIM model for those parameters to reveal the nature of chemical bonding in the considered Ge-doped lithium clusters. The electron density ($\rho(r_{BCP})$), Laplacian ($\nabla^2\rho(r_{BCP})$), bond ellipticity (ε), and the curvature λ_3 at the bond critical points (BCP) of the ground states of the neutral and cationic Li_nGe ($n = 1-5$) clusters are summarized in Table 4.

The Laplacian of ρ is the trace of the Hessian matrix of ρ, which has been used as a criteria to classify the interaction between atoms. When the Laplacian at the BCP $\nabla^2\rho(r_{BCP}) < 0$ and is large in absolute value, and the electron density $\rho(r_{BCP})$ itself is also large, the electronic charge is concentrated in the internuclear region, and the bond will be referred to as a shared interaction or covalent bond. In contrast, a positive Laplacian at the BCP suggests a closed-shell system. At the BCP of the closed-shell interaction, the electronic charge is depleted. In other words, these interactions are dominated by the contraction of electronic charge away from the interatomic surface toward the nuclei.

The ellipticity of a bond is a quantity defined as $\varepsilon = (\lambda_1/\lambda_2) - 1$ with the convention of $\lambda_1 \leq \lambda_2 \leq \lambda_3$, where λ_i are

eigenvalues of the Hessian matrix of ρ at a BCP. At a BCP, the electron density is a minimum along the bond path or $\lambda_3 > 0$, while there is a maximum along the other two perpendicular directions or λ_1, $\lambda_2 < 0$. The magnitudes of the eigenvalues indicate the curvature of the electron density along a given direction, while the ellipticity provides a measure of the π character of a bond.

From an AIM analysis on Li_nGe_2 ($n = 1-3$),[17] a very small covalent character has been attributed to the Li−Ge bond. Gatti et al.[32] found that in lithium clusters the lithium atoms are not bonded to one another but rather indirectly through a pseudoatom, which is actually a non-nuclear attractor. A pseudoatom exhibits the same topology as a real atom. The different point is that a pseudoatom is a true (3, −3) critical point rather than a cusp in electron density of a real nucleus. The loosely bound and delocalized electronic charge of a pseudoatom is responsible for the binding and conducting properties in lithium clusters.

The molecular graphs of the ground-state structures can be found in the Supporting Information. From $n = 1$ to 3, there is one BCP found between each Li and Ge atom; neither BCP nor non-nuclear attractor is found between Li atoms, even in the case of short distance between them such as in the quartet of Li_3Ge-C_{3v}, with a Li−Li distance of 2.749 Å (compare to 2.697 Å in Li_2 calculated at the same level). Combining with the ELF pictures of Li_3Ge and Li_3Ge^+ analyzed above, we can suggest that the presence of a Ge atom replaces the role of a pseudoatom in connecting Li atoms. The fact that the Laplacian of these BCPs is positive and relatively low (of the order of 10^{-2}) in value suggests closed-shell interactions between Ge and Li atoms. The electron densities at these BCPs are also low due to the contraction of electronic charge from BCPs. Thus, in these bonds the electronic charge concentrates on the basin of each atom, giving an ionic interaction.

A different picture of molecular graph was found for the Li_4Ge-rhombus. There are two direct bonds between Ge and equatorial Li atoms with the existence of BCP(Ge−Li_{eq}). The two axial Li atoms are not directly bonded with Ge, but through the pseudoatoms as found in pure Li clusters. Because the pseudoatom has no nucleus, it possesses a negative charge. The very small value of ρ at the pseudoatom suggests a delocalization of the electron around it. The Laplacian is negative and very small in value at the pseudoatom. The electron densities at BCPs in this case are smaller than at the BCP(Ge−Li) of smaller clusters. This can be explained by electron delocalization due to the existence of pseudoatom (denoted as Ps).

A familiar molecular graph returns for Li_5Ge C_{4v}. Here, there are five BCPs, one between Ge and axial Li and four between Ge and equatorial Li. The former bond has ellipticity of zero; it means that this bond has a cylindrical symmetry or σ character. The latter bonds have similar values of ρ and Laplacian but slightly larger ellipticity value, and this suggests a small π character of these bonds.

The pseudoatoms were found again in Li_5Ge^+ D_{3h}. In this cation, we found 3 Ps's, 6 ring, 3 cage, and 11 bond critical points. Two BCPs are found between Ge and axial Li atoms, three BCPs between equatorial Li and Ps, six BCPs between Ge and Ps, each Ps linking with Ge by two bonds. The ellipticity of the bond between Ge and pseudoatom is relatively high (1.32) due to the unbalance of two curvatures in interatomic surface, suggesting a high π character of these bonds.

For $Li_6Ge^{0,+}$, there are six BCPs around Ge. It is interesting that 7 BCPs between Ge and Li's were found in Li_7Ge^+, 6 BCP(Ge−Li) plus 1 BCP(Ge−Ps) and 1 BCP(Li−Ps) in Li_7Ge. So Ge can actually form seven bonds with Li's.

In summary, the Li−Ge bond in Li_nGe clusters is dominated by ionic character. Because of the small covalent character, Ge can make bonds with up to seven Li atoms. The Li atoms do not directly bond to each other, but rather through Ge or pseudoatoms.

Electron Shell Model. The electron shell model is a useful simple tool to predict and interpret the geometry, electronic structure, and stability of (spherical) metallic clusters.[33] It has been shown that most spherical clusters lead to the same progression of single particle levels, $1s^2/1p^6/1d^{10}2s^2/1f^{14}2p^6$..., corresponding to the magic numbers 2, 8, 18, 20, 34, 40... Each electron shell is characterized by a radial quantum number N and an angular quantum number L. For a doped cluster, the difference in electronegativity between host and dopant atoms must be taken into account, which leads to a modification of the ordering of the electronic levels. In the case of Ge-doped Li clusters, the central heteroatom is more electronegative than the host atom, and thereby the effective potential is more attractive at the center of the cluster. The orbitals that have most of their density in the center (i.e., s, and to a lesser extent p levels) will be energetically favored. As a result, energy levels of shells reverse, for example, the 1d/2s and 1f/2p level inversions, and then the level sequence becomes 1s/1p/2s/1d/2p/1f/....

The Li_6Ge cluster with an octahedral structure is a spherical cluster, and its 10 valence electrons are distributed in an orbital configuration as $a_{1g}^2t_{1u}^6a_{1g}^2t_{1u}^0t_{2g}^0e_g^0$.... The frontier MO's of Li_6Ge whose isosurfaces are fully shown in the Supporting Information describe a molecular configuration as $1s^21p^62s^22p^01d^0$. In the octahedral field of Li_6Ge, the 1d shell splits into two levels, t_{2g} including $1d_{xy}$, $1d_{yz}$, and $1d_{xz}$ orbitals, and e_g including $1d_{z2}$ and $1d_{x2-y2}$. In this case, the energy level of the 2p shell is pulled down even below the 1d shell. The fact that this has occurred is manifested in the large negative NBO charge on Ge (−3.65 e).

Applying the shell model with the modified series 1s/1p/2s/2p/1d for the $Li_nGe^{0,+}$ ($n = 1-7$), we can interpret the stability, favored spin states, and various gaps between low and high spin states of those clusters. Their number of valence electrons ranges from 4 to 11 in which two magic numbers of 8 and 10 can be found. The clusters with a magic number of electrons are Li_4Ge, Li_5Ge^+ (8 electrons), Li_6Ge, Li_7Ge^+ (10 electrons). In this context, they should be more stable than the others. Actually, Li_4Ge and Li_6Ge do show higher stability corresponding to the large HOMO−LUMO gaps. The Li_5Ge^+ and Li_7Ge^+ cations express the maxima in HOMO−LUMO gaps as well. It is interesting that these four clusters favor spherical-like geometries. For example, the Li_5Ge^+ ion prefers a trigonal bipyramid D_{3h} structure over the square pyramid C_{4v} of Li_5Ge. The Li_7Ge^+ ion, a monocapped octahedron, becomes much less prolate than the corresponding neutral by shortening the bond length between the capped Li and Ge centers (2.585 Å of cation vs 4.612 Å of neutral).

The investigated clusters clearly illustrate the transition from atoms to clusters with the structures dominated by the Ge orbitals. First, because of the ionic nature of the Li−Ge bonds and the absence of Li−Li bonds, these atomic orbitals are subsequently filled in going from $LiGe^+$ to Li_5Ge^+, or in going from $1s^21p^2$ to a filled $1s^21p^6$ configuration (corresponding to the electronic configuration of the Ge atom from $4s^24p^2$ to $4s^24p^6$). Here, the molecular orbitals of the cluster and the atomic orbitals of Ge basically coincide. Thus, as pointed out before, $LiGe^+$ is a complex between the Li^+ cation and Ge atom (Ge···Li^+), and Li_4Ge and Li_5Ge^+ have closed shells. For the next shell closure, the Li atoms

TABLE 5: Electron Configurations, Favored Spin States of Clusters with Different Numbers of Valence Electrons (*N*) Based on the Shell Model, and Corresponding Gaps (eV) between Low and High Spin States Calculated at B3LYP/aug-cc-pVTZ

				low−high spin state gap	
N	configuration	favored spin state	cluster	neutral	cation
4	$1s^21p^2$	triplet	$LiGe^+$		0.24
5	$1s^21p^3$	quartet	LiGe, Li_2Ge^+	0.29	0.31
6	$1s^21p^4$	triplet	Li_2Ge, Li_3Ge^+	0.42	0.04
7	$1s^21p^5$	doublet	Li_3Ge, Li_4Ge^+	0.66	0.04
8	$1s^21p^6$	singlet	Li_4Ge, Li_5Ge^+	0.76	1.36
9	$1s^21p^62s^1$	doublet	Li_5Ge, Li_6Ge^+	1.26	1.89
10	$1s^21p^62s^2$	singlet	Li_6Ge, Li_7Ge^+	0.51	0.76
11	$1s^21p^62s^22p^1$	doublet	Li_7Ge	0.57	

start to play an active role; forced by the configuration of the 4p(Ge) orbitals they form an octahedral structure, but the Li s-orbitals now form a 2s MO, giving in essence the next shell closure (Figure 3b). This leads to an electronically and configurationally quite stable Li_6Ge structure.

The favored spin state of these clusters can be understood by general rules of filling electron to shells such as Pauli's and Hund's rules. Accordingly, their preferential spin states as a function of the number of valence electrons are predicted and given in Table 5. The predictions of favored spin state based on this model are in excellent agreement with our extensive search for ground-state structures discussed above. For example, Li_3Ge possessing 7 valence electrons ($1s^21p^5$) is expected to favor a doublet state, whereas Li_3Ge^+ is having 6 electrons ($1s^21p^4$) and then favors a triplet state.

For the energy gaps between low and high spin states, there is a maximum at number of valence electrons $N = 9$ with the configuration of $1s^21p^62s^12p^0$. To form a quartet state, we need to excite one electron from the 1p shell to the 2p shell, and this process requires a large energy or a high gap. The second highest gap happens with $N = 8$ at which one electron has to be excited from the 1p to 2s shell to form a triplet state. The 1p−2s gap is smaller than the 1p−2p gap because the 2s shell energetically lies lower than the 2p shell and thus closer to the 1p shell.

4. Conclusions

In the present study, we carried out a combined experimental and theoretical investigation of the small neutral and cationic germanium doped lithium clusters $Li_nGe^{0,+}$ ($n = 1-7$). The clusters were unambiguously detected and characterized by time-of-flight mass spectrometry after laser vaporization and ionization. The molecular geometry and electronic structure of the doped clusters were investigated using quantum chemical calculations at the DFT/B3LYP and CCSD(T) levels with the aug-cc-pVnZ basis sets. The obtained results can be summarized as follows:

(i) The growth mechanism of the Ge-doped Li clusters appears to be clear. Their geometrical structures are built up based on the addition of Li, one by one, to Ge up to Li_6Ge, and then the seventh lithium atom starts capping to the face of the octahedron Li_6Ge. While $Li_3Ge^{0,+}$ and Li_4Ge^+ prefer planar geometry, the clusters from Li_4Ge to Li_7Ge and the corresponding cations, except for Li_4Ge^+, exhibit nonplanar geometries.

(ii) Clusters having from 4 to 6 valence electrons prefer high spin states, and low spin ground states are derived for the others because valence electron configurations are formed by filling electrons to the shells 1s/1p/2s/2p based on Pauli's and Hund's rules.

(iii) Because of the closed electronic shells, both the 8- and the 10-electron systems are more stable than the others. However, the 8-electron species is more favored than the 10-electron clusters. Apparently, the averaged binding energy for cation shows a maximum at Li_5Ge^+, which has the largest abundance in the experimental mass spectrum. This behavior is contrasting with the carbon-doped lithium clusters. The difference in atomic radii is the likely reason for why Ge does behave differently from C in their doped lithium clusters.

(iv) Li atoms do not bond to each other but through Ge or pseudoatoms, and an essentially ionic character can be attributed to the cluster chemical bonds.

(v) The adiabatic ionization energies are reduced upon increasing number of Li atoms. The value of $IE_a \approx 3.5$ eV represents one of the smallest values known so far for this quantity.

Acknowledgment. We are indebted to the KULeuven Research Council (GOA, IUAP, and IDO programs) for continuing support. V.T.N. and H.T.L. thank the Vietnam Government (MOET program 322) for doctoral scholarships.

Supporting Information Available: Figures showing spin densities, frontier molecular orbitals, ELF isosurfaces, molecular graphs, and Cartesian coordinates of the optimized structures. This material is available free of charge via the Internet at http://pubs.acs.org.

References and Notes

(1) (a) Wu, C. H. *J. Chem. Phys.* **1976**, *65*, 3181. (b) Wu, C. H. *J. Phys. Chem.* **1983**, *87*, 1534.

(2) Sarkas, H. W.; Arnold, S. T.; Hendrickx, J. H.; Bowen, K. H. *J. Chem. Phys.* **1995**, *103*, 2653.

(3) (a) Dugourd, Ph.; Blanc, J.; Bonacic-Koutecky, V.; Broyer, M.; Chevaleyre, J.; Koutecky., J.; Pittner, J.; Wolf, J. P.; Woste, L. *Phys. Rev. Lett.* **1991**, *67*, 2638. (b) Blanc, J.; Bonacic-Koutecky, V.; Broyer, M.; Chevaleyre, J.; Dugourd, Ph. *J. Chem. Phys.* **1992**, *96*, 1793.

(4) Brechignac, C.; Busch, H.; Cahuzac, Ph.; Leygnier, J. *J. Chem. Phys.* **1994**, *101*, 6992.

(5) (a) Rao, B. K.; Khanna, S. N.; Jena, P. *Phys. Rev. B* **1987**, *36*, 953. (b) Gardet, G.; Rogemond, F.; Chermette, H. *J. Chem. Phys.* **1996**, *105*, 9933. (c) Fournier, R.; Joey, Cheng, J. B. Y.; Wong, A. *J. Chem. Phys.* **2003**, *119*, 9444. (d) Wheeler, S. E.; Sattelmeyer, K. W.; Schleyer, P. v. R.; Schaefer, H. F.; Wu, C. H. *J. Chem. Phys.* **2004**, *120*, 4683. (e) Temelso, B.; Sherrill, C. D.; Wu, C. H. *J. Chem. Phys.* **2005**, *122*, 064315, and references therein.

(6) Shaik, S.; Hiberty, P. C. *J. Am. Chem. Soc.* **1985**, *107*, 3089.

(7) (a) Wu, C. H.; Kudo, H.; Ihle, H. R. *J. Chem. Phys.* **1979**, *70*, 1534. (b) Wu, C. H. *Chem. Phys. Lett.* **1987**, *139*, 357.

(8) Kudo, H. *Nature* **1992**, *355*, 432.

(9) Li, Y.; Wu, D.; Li, Z. R.; Sun, C. C. *J. Comput. Chem.* **2007**, *28*, 1677.

(10) Jones, R. O.; Lichtenstein, A. I.; Hutter, J. *J. Chem. Phys.* **1997**, *106*, 4566.

(11) Lee, M. S.; Gowtham, S.; He, H.; Lau, K. C.; Pan, L.; Kanhere, D. G. *Phys. Rev. B* **2006**, *74*, 245412.

(12) Lievens, P.; Thoen, P.; Bouckaert, S.; Bouwen, W.; Vanhoutte, F.; Weidele, H.; Silverans, R. E.; Navarro-Vazquez, A.; Schleyer, P. v. R. *Eur. Phys. J. D* **1999**, *9*, 289.

(13) (a) Joshi, K.; Kanhere, D. G. *Phys. Rev. A* **2002**, *65*, 043203. (b) Shetty, S.; Pal, S.; Kanhere, D. G. *J. Chem. Phys.* **2003**, *118*, 7288.

(14) Lievens, P.; Thoen, P.; Bouckaert, S.; Bouwen, W.; Vanhoutte, F.; Weidele, H.; Silverans, R. E.; Navarro-Vazquez, A.; Schleyer, P. v. R. *J. Chem. Phys.* **1999**, *110*, 10316.

(15) Lievens, P.; Thoen, P.; Bouckaert, S.; Bouwen, W.; Vanhoutte, F.; Weidele, H.; Silverans, R. E. *Chem. Phys. Lett.* **1999**, *302*, 571.

(16) Bouwen, W.; Thoen, P.; Vanhoutte, F.; Bouckaert, S.; Despa, F.; Weidele, H.; Silverans, R. E.; Lievens, P. *Rev. Sci. Instrum.* **2000**, *71*, 54.

(17) Gopakumar, G.; Lievens, P.; Nguyen, M. T. *J. Chem. Phys.* **2006**, *124*, 214312.
(18) Yannouleas, C.; Landman, U. *Phys. Rev. B* **1995**, *51*, 1902.
(19) (a) Gopakumar, G.; Lievens, P.; Nguyen, M. T. *J. Phys. Chem. A* **2007**, *111*, 4355. (b) Gopakumar, G.; Wang, X.; Lin, L.; De Haeck, J.; Lievens, P.; Nguyen, M. T. *J. Phys. Chem. C* **2009**, *113*, 10858.
(20) Neukermans, S.; Janssens, E.; Tanaka, H.; Silverans, R. E.; Lievens, P.; Yokoyama, K.; Kudo, H. *J. Chem. Phys.* **2003**, *119*, 14.
(21) Becke, A. D. *J. Chem. Phys.* **1996**, *104*, 1040. Lee, C. T.; Yang, W. T.; Parr, R. G. *Phys. Rev. B* **1988**, *37*, 785.
(22) Dunning, T. H., Jr. *J. Chem. Phys.* **1989**, *90*, 1007. Kendall, R. A.; Dunning, T. H., Jr.; Harrison, R. J. *J. Chem. Phys.* **1992**, *96*, 6796.
(23) Barlett, R. J.; Musia, M. *Rev. Mod. Phys.* **2007**, *79*, 291.
(24) Frisch, M. J.; Trucks, G. W.; Schlegel, H. B.; Scuseria, G. E.; Robb, M. A.; Cheeseman, J. R.; Montgomery, J. A., Jr.; Vreven, T.; Kudin, K. N.; Burant, J. C.; Millam, J. M.; Iyengar, S. S.; Tomasi, J.; Barone, V.; Mennucci, B.; Cossi, M.; Scalmani, G.; Rega, N.; Petersson, G. A.; Nakatsuji, H.; Hada, M.; Ehara, M.; Toyota, K.; Fukuda, R.; Hasegawa, J.; Ishida, M.; Nakajima, T.; Honda, Y.; Kitao, O.; Nakai, H.; Klene, M.; Li, X.; Knox, J. E.; Hratchian, H. P.; Cross, J. B.; Bakken, V.; Adamo, C.; Jaramillo, J.; Gomperts, R.; Stratmann, R. E.; Yazyev, O.; Austin, A. J.; Cammi, R.; Pomelli, C.; Ochterski, J. W.; Ayala, P. Y.; Morokuma, K.; Voth, G. A.; Salvador, P.; Dannenberg, J. J.; Zakrzewski, V. G.; Dapprich, S.; Daniels, A. D.; Strain, M. C.; Farkas, O.; Malick, D. K.; Rabuck, A. D.; Raghavachari, K.; Foresman, J. B.; Ortiz, J. V.; Cui, Q.; Baboul, A. G.; Clifford, S.; Cioslowski, J.; Stefanov, B. B.; Liu, G.; Liashenko, A.; Piskorz, P.; Komaromi, I.; Martin, R. L.; Fox, D. J.; Keith, T.; Al-Laham, M. A.; Peng, C. Y.; Nanayakkara, A.; Challacombe, M.; Gill, P. M. W.; Johnson, B.; Chen, W.; Wong, M. W.; Gonzalez, C.; Pople, J. A. *Gaussian 03*, revision B.03; Gaussian, Inc.: Wallingford, CT, 2003.
(25) (a) Bader, R. F. *Atoms in Molecules A Quantum Theory*; Oxford University Press: New York, 1995. (b) Popelier, P. *Atoms in Molecules. An Introduction*; Prentice Hall: New York, 2000.
(26) (a) Becke, A. D.; Edgecombe, K. E. *J. Chem. Phys.* **1990**, *92*, 5397. (b) Silvi, B.; Savin, A. *Nature* **1994**, *371*, 683. (c) Kohout, M. *Int. J. Quantum Chem.* **2004**, *97*, 651. (d) Kohout, M.; Wagner, F. R.; Grin, Y. *J. Phys. Chem. A* **2002**, *108*, 150.
(27) Biegler-König, F.; Schönbohm, J.; Bayles, D. AIM2000 - A Program to Analyze and Visualize Atoms in Molecules. *J. Comput. Chem.* **2001**, *22*, 545.
(28) Noury, S.; Krokidis, X.; Fuster, F.; Silvi, B. *TopMod package*; Université Pierre et Marie Curie: Paris, France, 1998.
(29) (a) Laaksonen, L. J. *J. Mol. Graphics* **1992**, *10*, 33. (b) Bergman, D. L.; Laaksonen, L.; Laaksonen, A. *J. Mol. Graphics Model.* **1997**, *15*, 301.
(30) Reed, A. E.; Schleyer, P. v. R.; Janoschek, R. *J. Am. Chem. Soc.* **1991**, *113*, 1885.
(31) (a) Marsden, C. J. *Chem. Phys. Lett.* **1995**, *245*, 475. (b) Schleyer, P. v. R.; Kapp, J. *Chem. Phys. Lett.* **1996**, *255*, 363.
(32) Cao, W. L.; Gatti, C.; Macdougall, P. J.; Bader, R. F. W. *Chem. Phys. Lett.* **1987**, *141*, 380.
(33) Janssens, E.; Neukermans, S.; Lievens, P. *Curr. Opin. Solid State Mater. Sci.* **2004**, *8*, 185, and references therein.

JP9056913